Performance of overpass structures with reinforced earth walls in the Kaikoura earthquake

John Wood[1], D. Asbey-Palmer[2], and G. Power[3]

[1] John Wood Consulting, 20A Ngaumatau Rd, Lower Hutt, 5013, New Zealand
[2] The Reinforced Earth Company, 218/13 Laidlaw Way. Auckland, 2019, New Zealand
[3] The Reinforced Earth Company, 20 George Street, Hornsby, NSW, 2077, Australia

ABSTRACT

The paper presents earthquake performance assessments of the Seddon and Hawkswood Railway Overbridges that were subjected to strong ground shaking in the November 2016 Kaikoura Earthquake. Both structures are located on the main State Highway in the north-eastern region of the South Island of New Zealand (NZ). Their performance was of interest because of the dominance of geotechnical aspects in their design. The Seddon Overbridge is a single-span bridge that has spread footing abutments sitting directly on Reinforced Earth® (reinforced fill, RF) walls. The Hawkswood Overbridge, is a TechSpan® buried three-hinged arch constructed from reinforced precast concrete segments. Headwalls to the arch are of similar RF construction to the Seddon Overbridge walls. Back-analyses based on recorded input ground motions predicted the good performance of both overbridges in the strong shaking.

Keywords: Reinforced Earth®; Techspan®; reinforced fill; buried arch structures; earthquake performance; bridges

1. INTRODUCTION

The 14 November 2016, M_w 7.8, Kaikoura earthquake had an epicentre located 62 km south-west of the town of Kaikoura on the northern part of the east coast of the South Island of NZ. Ruptures occurred on multiple fault lines in a complex sequence that resulted in strong shaking over a wide area. Landslides closed the main State Highway (SH 1) and adjacent Main Trunk Railway for approximately one year. One bridge on a local road collapsed and 28 SH bridges received significant damage (Wood and McHaffie 2017, 2018).

The region surrounding the Hawkswood and Seddon Railway Overbridges is serviced by 15 strong-motion accelerographs that are part of the NZ GeoNet hazard monitoring system. The proximity of the recording stations to the overbridges enabled a good estimate to be made of the ground motions at the bridge sites and this provided the basis for back-analyses to determine whether the minor cracking in the Hawkswood arch and small displacements observed in the RF walls of both bridges could be predicted by calculation methods used in design.

Bridges supported directly on RF abutment walls and underground concrete arch structures have not previously been subjected to the intensity of shaking experienced in the Kaikoura earthquake. The peak ground acceleration (PGA) recorded near the Seddon Overbridge was 0.74 g. A PGA of 0.6 g was estimated for the Hawkswood Overbridge site.

2. SEDDON RAILWAY OVERBRIDGE

2.1 Bridge Details

The Seddon Railway Overbridge, constructed in 1991, is an 18 m long single-span bridge with a superstructure constructed of ten pretensioned double hollow core beam units. Reinforced concrete (RC) spread footing abutment beams sit directly on the RF.

Both abutment walls have a height of 7.7 m measured from the top of the wall facing foundation to the road surface on the centre-line of the bridge. The wall facings are constructed of cruciform shaped precast 180 mm thick reinforced concrete panels with height and width dimensions of 1.5 m. Galvanised, hot-rolled ribbed 60 x 5 mm steel strips, connected to the facing panels, and varying in length from 7 m at the

base with 4 strips/3 m width to 10 m at the top with 11 strips/3 m width were used to create the RF.

The structural arrangement is shown in Figure 1 and a typical section through the main abutment walls is shown in Figure 2.

Site investigations showed one metre of loess and fill overlying dense sand and gravels with mudstone at a depth of 2 to 3 m below the ground surface. The loess and fill were removed before construction of the wall foundations and the embankments for the bridge approaches. Select granular soil with a minimum density of 18 kN/m^3 was used in the RF.

Figure 1. Seddon Railway Overbridge.

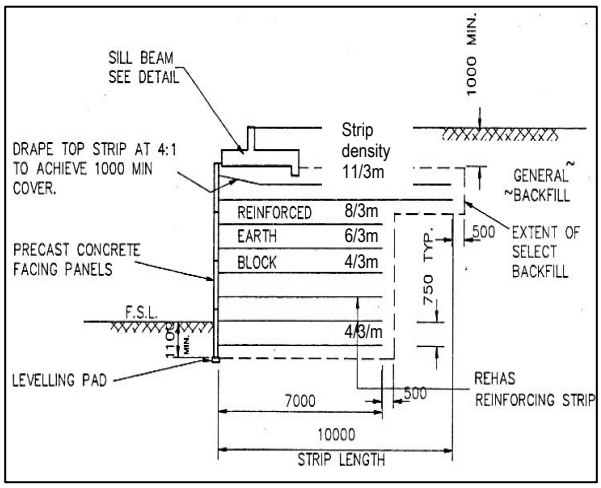

Figure 2. Seddon Railway Overbridge. Abutment section.

2.2 Bridge Performance

Minor spalling and cracking were evident on the corners of five of the panels on the south abutment wall. There was minor rotation of the facing panels and some permanent outward displacement on this wall. A gap of 35 mm developed between the abutment wall facing and the vertical face of the toe of the abutment footing at the west end. The extent of the facing damage and the outward displacement of the footing are shown in Figures 3 and 4.

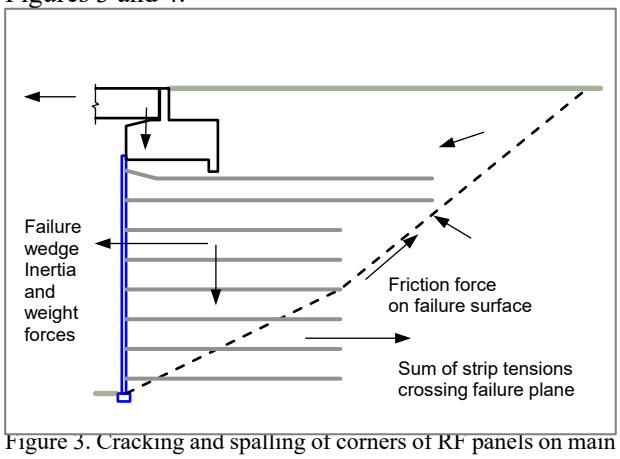

Figure 3. Cracking and spalling of corners of RF panels on main south abutment wall.

Figure 4. Gap of 35 mm between top of wall and abutment footing at west side of south abutment.

2.3 Bridge Analysis

Acceleration time-histories recorded in the Kaikoura Earthquake at the Seddon Fire Station (SEDS) GeoNet recording station located 200 m from the site were used in the back-analyses. The recording station V_s30 average shear wave velocity and the depth to bedrock (shear wave velocity V_s = 1,000 m/s) have been assigned as 270 m/s and 50 m respectively. These site parameters were based on geological maps as no site investigation has been carried out at the recording station. At the bridge site there was mudstone at a depth of 2 to 3 m below the ground surface. Shear wave velocities for mudstone range from 600 to 800 m/s so the depth to V_s = 1,000 m/s was probably greater at the recording site than at the bridge site.

The recorded accelerations were resolved into the longitudinal and transverse principal directions of the bridge using trigonometric vector relationships.

The back-analysis work focused on the longitudinal response of the bridge and the abutment walls. The ground acceleration level to initiate a sliding failure within the RF at the abutments, and the transfer of the bridge inertia forces into the RF were investigated.

A limiting equilibrium method (Bracegirdle, 1980) was used to predict the critical response acceleration to initiate sliding movement in the RF abutments. A bilinear failure surface is assumed to develop at the toe of the wall and to propagate up through the RF and the retained soil behind the RF. An upper-bound failure criterion is applied to find the critical failure surface inclination angles and the acceleration at which sliding develops. The disturbing forces acting on the sliding block are the imposed forces from the bridge, RF soil weight and inertia force, and the Mononobe-Okabe (M-O) pressure on the back of the RF (Wood and Elms, 1990). These are resisted by soil friction on the failure surface and the tension forces in the reinforcing strips that cross the failure surface. Figure 5 shows the location of the forces acting on the failure wedge.

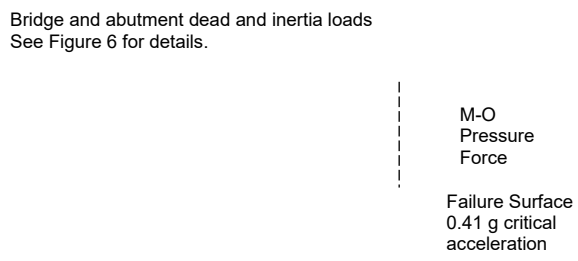

Figure 5. Forces acting on failure wedge within RF abutments.

Outward displacement on the failure surface was calculated using the longitudinal direction acceleration time-history as input to a Newmark (1965) sliding block analysis.

Under loads directed away from the abutment backfill (pull abutment) the inertia forces are resisted by sliding friction on the base of the footing. Friction forces are then transferred to the facing panels which resist these outward pressures by load transfer to the reinforcing strips anchoring the panels to the top of the RF (typically the top two layers of strips). At the opposite abutment, the inertia forces are resisted by combined passive resistance of the abutment backwall and sliding friction on the base of the footing. Forces acting on the pull abutment are shown in Figure 6. Forces acting on the opposite abutment are similar with the active soil pressure replaced by a passive soil pressure resistance.

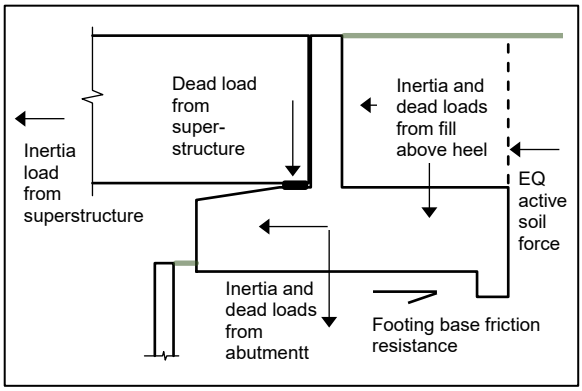

Figure 6. Forces acting on pull abutment.

The passive stiffness and strength capacity of the soil retained by the abutment back face (2 m total height) was calculated using a hyperbolic backbone curve from Kahalili-Tehrani et al, (2010). The strength capacity was verified using the LimitState:GEO software (http://www.limitstate.com/geo).

The main parameters used in the analyses are listed in Table 1. Probable strengths were used for the soil and structural materials rather than design values.

Table 1. Parameters used in back analysis.

Parameter	Value
Total weight of superstructure	2,800 kN
Weight of each abutment structure	1,000 kN
Weight of soil on abutment heel	280 kN
Total gravity reaction at base of footings	200 kN/m
Unit weight of soil in RF block	20 kN/m^2
Soil friction angle in RF block	36^o
Soil friction angle in general backfill	36^o
RF strip friction factor at surface	2.25
RF strip friction factor at 6 m depth	1.09
RF strip yield stress	275 MPa

2.4 Analysis Results

Critical accelerations to initiate outward sliding in the abutment RF and the highest wing wall section were 0.41g and 0.35 g respectively. The failure acceleration in the abutment RF was based on assuming one-half of the bridge inertia load was transferred to each abutment. More detailed analysis of the soil stiffness at either abutment indicated that this was a satisfactory approximation. Figure 5 shows the location of predicted failure surface in the abutment RF.

Under the longitudinal time-history (PGA of 0.68 g) the Newmark analysis predicted a sliding displacement of 10 mm for the combined mass of the superstructure, abutment structure and RF failure wedge. Figure 7 shows the input acceleration history and the calculated displacement function. Most of the displacement occurred in three strong acceleration peaks near the end of the input record.

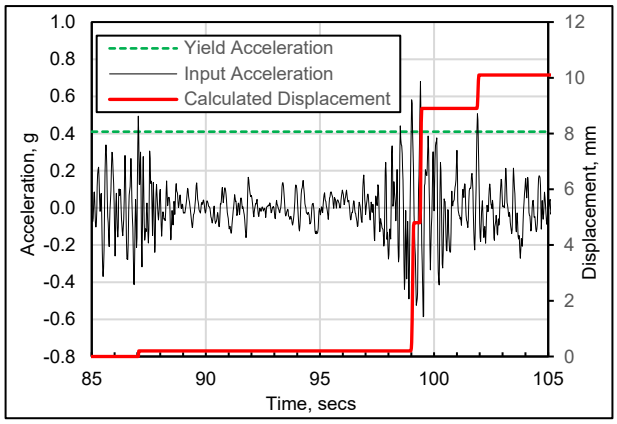

Figure 7. Newmark sliding block input acceleration and output displacement.

To check the sensitivity of the calculated displacement to the critical acceleration the yield level was reduced by 10% resulting in the displacement increasing to 17 mm.

The passive capacity of the abutment footing walls estimated using both the backbone curve method and LimitState:GEO was 250 kN per metre of width. The analysis of the transfer of the abutment and bridge loads into the RF indicated that the friction on the base of the footings would resist about 95% of the total inertia load from the superstructure and abutment footings, (including the active pressure component on the pull abutment back wall). The additional load of approximately 15 kN/m would be resisted by passive pressure against the footing backwall following sliding movements of a few millimetres.

The facing panels and top strips had adequate strength to transfer the estimated friction forces from the base of the footings into the RF.

2.5 Concluding Comments

The analyses indicated that small movements of the bridge could be expected. The 35 mm gap that was

observed to have opened between the abutment wall and the footing at the south abutment appeared to be from outward displacement of the facing rather than the overall movement of the bridge and abutments. Outward movement of the west wing wall may have been a factor as its critical acceleration was lower than for the main walls.

Good performance was achieved with the abutment footings directly on top of the RF without piles.

3. Hawkswood Railway Overbridge

3.1 Bridge Details

The Hawkswood Railway Overbridge, constructed in stages between 1999 and 2001, is a 42 m long TechSpan® buried arch with an average soil cover of 1.4 m. Precast RC arch segments, 2.0 m wide by 200 mm thick, were assembled in two halves to form a three-hinged arch 6.7 m wide by 5.2 m high with a shape designed to be a funicular curve under gravity loading. The arch is founded on 1.5 m wide by 400 mm deep RC strip footings.

Headwalls to the arch barrel are of similar RF construction to the Seddon Overbridge abutment walls. Their maximum height and length are 6.7 m and 17.7 m respectively. The steel strips have a length of 5.8 m and a section of 45 x 5 mm.

The arch and wing walls are shown in Figure 8. Typical sections are shown in Figures 9 and 10.

Figure 8. Hawkswood Railway Overbridge. Looking to south.

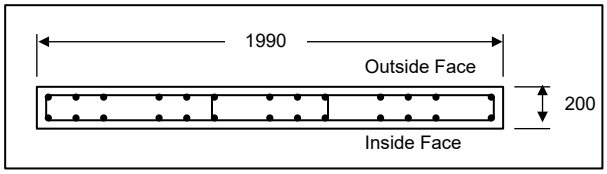

Figure 9. Arch section. Reinforcement at mid-section (Sect. A). Main bars: D12 Grade 430. Stirrups: R10 Grade 300 at 150mm centres.

The soil on the edge of the railway cutting contained clayey silt with gravel adjacent to the angular ballast making up the railway track bed. This was underlain by firm silt over dense sand and gravel.

The footings were designed for an allowable bearing pressure of 350 kPa.

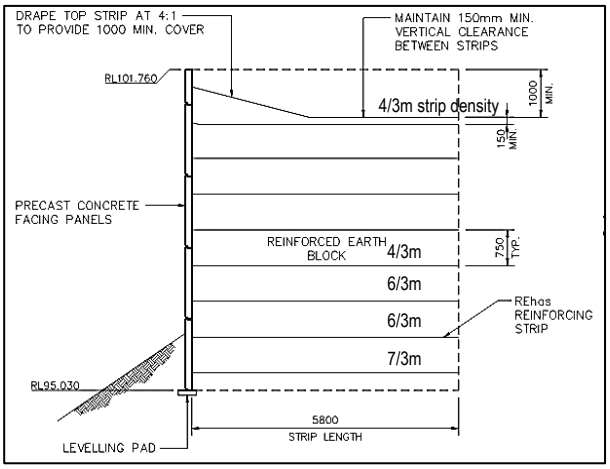

Figure 10. Section of wing walls at maximum height.

3.2 Bridge Performance

Fine inclined cracks were present at the base of several of the arch units at the northwest corner; a location with low axial load. These may have been caused by longitudinal earthquake loading. Joint gaps between adjacent units could have resulted in the units acting separately making them more susceptible to damage than would be the case for a more integral structure.

Facing panels in the northeast wingwall experienced some rotation and dislocation (see Figure 11). A depression in the road surface behind this section of wall indicated minor outward movement of the top of the wall. There was no damage to the panels in the other wingwalls.

3.3 Ground Motions

The overbridge lies approximately 24 km east of the epicentre of the Kaikoura Earthquake. Two strong-motion accelerographs were located within 22 km of the overbridge site. These recorded PGA's of 0.29 g

and 0.99 g. The intensity of shaking at site would have been intermediate between these two values and based on the proximity and direction of rupture of the nearest causative fault probably at the higher end of the range.

Figure 11. North-east wing wall. Spalling damage and minor misalignment of panels.

3.4 Analysis of Arch and Walls

A two-dimensional plane-strain finite element analysis (FEA) was carried out on a typical arch section using soil strength and stiffness parameters based on hyperbolic shear stress-strain relations given in Duncan et al, (1980). The arch structure was represented by elastic two-dimensional beam elements. Gravity and earthquake load actions in the arch were calculated separately using a nonlinear analysis model that incorporated contact elements between the soil and arch structure.

A section of the FEA model is shown in Figure 12. Boundary conditions were modified between the gravity and earthquake load cases to enable only one-half of the arch to be analysed. Under earthquake loading the vertical boundaries were assumed to be free to translate in the x-axis direction and to rotate about the z-axis. For gravity loading these boundaries were free to translate in the y-axis direction but were restrained in the other translational and all three rotational directions. Gravity load actions were calculated using superimposed incremental loads resulting from construction of the backfill in 0.5 m thick layers. To model different layer depths that might arise on either side of the arch during construction a full-arch model is required but the simplification used in the present study was satisfactory considering the uncertainty in the soil properties (no test results were available for the backfill soil).

The earthquake load was applied as a uniform horizontal body force acting on the foundation and backfill soil, and the concrete arch. The magnitude was taken as $C_o\gamma$, where C_o is the earthquake acceleration coefficient and γ the unit weight of the soil or concrete.

Figure 12. FEA mesh used for the analysis of the arch section.

A summary of the material properties is given in Table 2. Probable strengths were used for the arch and soil properties rather than design values.

The wing walls were analysed using the procedures described for the Seddon Overbridge RF abutments.

Table 2. Parameters used in arch analysis.

Parameter	Value
Arch reinforcement yield stress	475 MPa
Arch concrete compression strength	52 MPa
Young's modulus for concrete	34 GPa
Arch section area	0.2 m^2/m
Arch moment of inertia for Gravity loading	0.00067 m^4/m
Arch cracked moment of inertia for EQ loading	0.00033 m^4/m
Soil unit weight	22 kN/m^3
Soil friction angle	39°
Modulus number (Duncan et al, K)	450
Modulus exponent (Duncan el al, n)	0.4
Bulk modulus number (Duncan et al, Kb)	200
Bulk modulus exponent (Duncan et al, m)	0.2
Initial tangent modulus top layer	28 MPa
Initial tangent modulus bottom backfill layer	51 MPa
Initial tangent modulus foundation soil	60 MPa
Final tangent modulus top layer	27 MPa
Final tangent modulus bottom backfill layer	44 MPa
Final tangent modulus foundation soil	60 MPa
Contact element friction coefficient	0.5
Thickness of construction layers	0.5 m

3.5 Analysis Results

Bending moments (BMs) and axial forces in the arch for combined gravity (G) and an 0.6 g earthquake (E) load are shown in Figure 13. To assess the arch performance, corresponding BM and axial force values shown in Figure 13 were plotted on the yield capacity chart shown in Figure 14. The plotted yield capacity is the capacity when the bars commence to yield rather than the ultimate or fully plastic moment capacity.

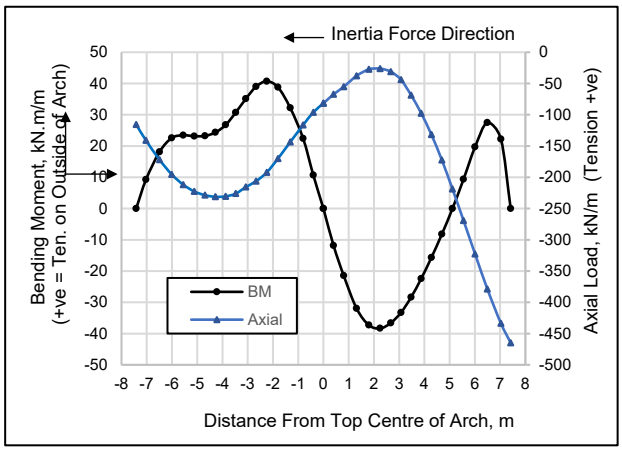

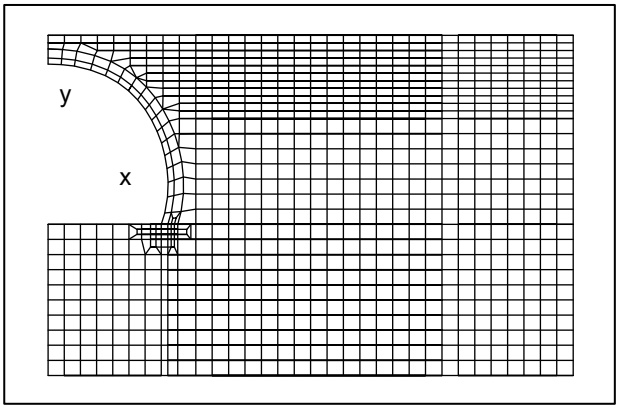

Figure 13. Force actions under G + 0.6 g E load.

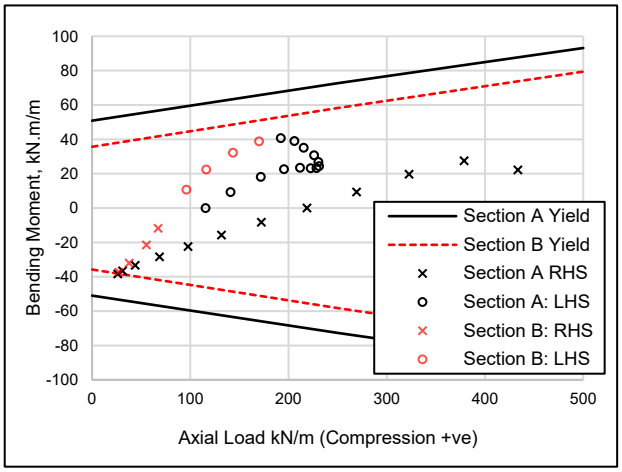

Figure 14. G + 0.6g E actions and arch yield capacity lines.

Section A in Figure 14 has the reinforcement details shown in Figure 9. Section B is a section near the top and bottom of the arch segments where four of the 13 bars on each face are discontinued. Figure 13 shows that the most critical section is at a location 1.8 m from the top centre of the arch (Section B reinforcement) where the G + E moment is -37 kN.m/m (tension on inside of arch) and the axial compression is 27 kN/m. These actions result in reinforcement yield at this location. However, inspection following the earthquake did not indicate any significant cracking at the critical section.

The critical acceleration to initiate outward failure in the highest wingwall section was 0.37 g. Since there were no ground motions recorded close to the site the outward displacements were estimated by the Jibson (2007) correlation equation (derived from Newmark sliding block analyses). For an assumed PGA of 0.6 g, a critical acceleration of 0.4 g, and a 10% probability of exceedance the estimated displacement was 21 mm. For a 50% probability of exceedance this value reduced to 6 mm. A check was made on the Jibson equation displacements by carrying out a sliding block analysis using the SEDS Kaikoura Earthquake record used for the analysis of the Seddon Overbridge scaled to a PGA of 0.6 g. This gave a displacement of 10 mm which was within the limits of the Jibson equation predictions. Minor misalignment of some of the panels indicated that outward sliding of the order of 10 to 20 mm may have occurred.

3.6 Concluding Comments

For an assumed site PGA of 0.6 g analyses based on methods used in design gave a good prediction of the observed performance of the arch; however, the results of the analyses were found to be sensitive to assumptions made on the backfill stiffness and the degree of cracking in the arch structure. There is also uncertainty in the intensity of shaking and in the distribution of the inertia forces acting in the soil mass surrounding the structure.

The observed minor cracking in the arch and the wing wall misalignment had no detrimental structural effect.

ACKNOWLEDGEMENTS

Funding was provided by the NZ Transport Agency and The Reinforced Earth Company (REC).

Jeremy Waldin and Mark Jeffries of WSP-Opus provided information on the damage and bridge details. Chris Lawson of REC supplied drawings and reviewed the paper. Their input provided invaluable assistance.

REFERENCES

Bracegirdle A. (1980). Seismic Stability of Reinforced Earth Retaining Walls. Bulletin NZSEE, Vol. 13 (4).

Duncan J. M., Byrne P., Wong K. S. and Mabry P. (1980). Strength, Stress-Strain and Bulk Modulus Parameters for Finite Element Analyses of Stress and Movements in Soil Masses. Report No UCB/CT/80-01, UC, Berkley.

Jibson R. W. (2007). Regression Models for Estimating Coseismic Landslide Displacement. Engineering Geology Vol 91, Issues 2-4, pp. 209-218.

Kahalili-Tehrani P., Taciroglu E., and Shamsadadi A. (2010). Backbone Curves for Passive Response of Walls with Homogenous Backfills. Soil-Foundation-Structure Interaction, Taylor & Francis Group, London.

Newmark N. M. (1965). Effects of Earthquakes on Dams and Embankments, Geotechnique, XV (2).

Wood J. H. and Elms D. G. (1990). Seismic Design of Bridge Abutments and Retaining Walls. RRU Bulletin 84, Vol. 2. Transit New Zealand.

Wood J. H. and McHaffie B. (2017). Performance of State Highway Bridges in the Kaikoura Earthquake: Five Bridges Located near the Epicentre at Waiau. Report prepared for NZ Transport Agency.

Wood J. H. and McHaffie B. (2018). Performance of State Highway Bridges in the Kaikoura Earthquake: Five Bridges Located Between Seddon and Kaikoura. Report prepared for NZ Transport Agency